

# Clocked Hysteresis Control Scheme With Power-Law Frequency Scaling in Buck Converter to Improve Light-Load Efficiency for IoT Sensor Nodes

Chung-Shiang Wu<sup>1</sup>, *Student Member, IEEE*, Makoto Takamiya, *Senior Member, IEEE*,  
and Takayasu Sakurai, *Fellow, IEEE*

**Abstract**—A clocked hysteresis control scheme with power-law frequency scaling is proposed to improve the conversion efficiency at a light load current, and it is applied to a buck converter design. By replacing a continuously on comparator used in conventional hysteresis control by a clocked comparator with power-law frequency scaling, the buck converter consumes no direct current (dc) in the comparators. Almost flat efficiency over a load current ranging from 500 nA to 20 mA is achieved. In addition, a quick wakeup feature is maintained because of the inherent hysteresis control. As for the theoretical aspect, expressions for the frequency stability condition, power consumption, and output voltage ripple of the proposed power-law frequency scaling scheme are derived and analyzed. A leakage-based digitally controlled oscillator, which consumes only 3.5 nW when the frequency is 15 Hz for 500-nA load current, is designed to provide a clock signal to the clocked comparator. Experimental results show that the buck converter implemented with the power-law frequency scaling scheme achieves a 90.4% peak efficiency and higher than 87% efficiency over a load current range from 500 nA to 20 mA.

**Index Terms**—Clocked hysteresis control (CHC), discontinuous conduction mode (DCM) buck converter, hysteresis control, power-law frequency scaling, wide-load-range buck converter.

## I. INTRODUCTION

WITH the rapid growth of Internet-of-Things (IoT) applications, demand for the development of wireless sensor nodes is increasing. Many applications such as smart cities/buildings, healthcare, and even those in industrial fields require sensors operating for a long time without the need to replace the battery. A direct current to direct current (dc–dc) converter used in IoT sensor nodes to convert the battery input voltage to a well-regulated output voltage for large-scale integrated (LSI) circuits should provide a high conversion efficiency to prolong the battery lifetime. Unlike mobile applications, the wireless sensors employed in IoT applications stay in a sleep mode for most of the time and quickly wake up to transmit data for only a short period of time. It has

been shown by calculation [1] that the energy consumption of the sleep mode is 10 times that of the active mode when the sleep current is 1  $\mu$ A, as specified in the Bluetooth low energy (BLE) specifications [2]. Therefore, the conversion efficiency in the sleep mode is becoming increasingly important to reduce overall energy consumption.

Thus far, several commercial products and publications on buck converters for IoT sensor node applications have been reported. The conversion efficiency, however, degrades rapidly when the load current decreases to microampere order [3]. A tri-mode buck converter consisting of a digital pulsewidth modulation, a pulse-frequency modulation (PFM), and an asynchronized mode (AM) [4] improves the conversion efficiency and extends the possible load range to 100 nA. The conversion efficiency, however, is still lower than 80% when the converter operates in the AM for a 1- $\mu$ A load. An adaptive application of bias current for analog circuits depending on the loading conditions [5] improves the conversion efficiency when the load current is low. The quiescent current in [5] was as low as 110 nA with low output voltage ripple performance. The conversion efficiency, however, was still limited to 78% when the load current was 1  $\mu$ A. In contrast, the buck converter proposed in [6] achieved 87% conversion efficiency at 1  $\mu$ A, but it did not supply sufficient load current in an active mode and did not support a fast wakeup operation required for IoT applications.

For IoT applications, because of the low load current in a sleep mode and a limited area for an inductor, the buck converter operating in a discontinuous conduction mode (DCM) is required. There are two basic control schemes for a buck converter operating in the DCM: constant-on-time (COT) control and hysteresis control. These two schemes are shown in Fig. 1(a) and (b), respectively. In COT control [7], a high-speed comparator is employed to compare the output voltage with a reference voltage  $V_{REF}$ . A pulse signal with a fixed pulsewidth is applied to the power stage triggered by the comparator output signal. The output voltage is regulated as  $V_{OUT} = V_{REF}$ , and the voltage error between  $V_{REF}$  and  $V_{OUT}$  is monitored continuously. On the other hand, hysteresis control uses hysteresis comparators to regulate the output voltage within a designed hysteresis voltage window. In addition, hysteresis control inherently provides a high

Manuscript received September 13, 2017; revised December 20, 2017; accepted January 25, 2018. Date of publication March 8, 2018; date of current version May 22, 2018. (Corresponding author: Chung-Shiang Wu.)

The authors are with the Institute of Industrial Science, University of Tokyo, Tokyo 153-8505, Japan (e-mail: cswu@iis.u-tokyo.ac.jp; mtaka@iis.u-tokyo.ac.jp; tsakurai@iis.u-tokyo.ac.jp).

Color versions of one or more of the figures in this paper are available online at <http://ieeexplore.ieee.org>.

Digital Object Identifier 10.1109/TVLSI.2018.2806928

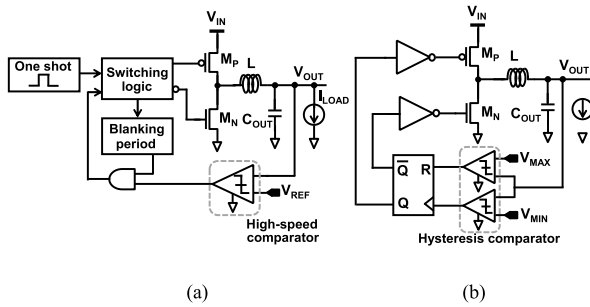


Fig. 1. Conventional control schemes for buck converter operating in DCM. (a) COT control. (b) Hysteresis control.

output voltage response speed when  $I_{LOAD}$  changes [8]. This is preferable, especially in IoT applications when a quick wake-up operation is required to conserve the energy of a system. Both schemes, however, consume dc current because they require continuously on comparators to monitor the output voltage. A typical circuit schematic of the continuously on comparator in Fig. 1(a) and (b) is shown in Fig. 2(a) [9], [10]. To clarify the power distribution of the typical hysteresis buck converter shown in Fig. 1(b), a simulation assuming that  $V_{IN}$  is 3 V and  $V_{OUT}$  is 1.6 V with a 20-mV hysteresis voltage window and 1- $\mu$ A bias current is conducted. Fig. 3(a) shows the power distribution in a sensor node in an active mode when  $I_{LOAD}$  is 10 mA. In a sleep mode where  $I_{LOAD}$  is 1  $\mu$ A, as specified by BLE, the power consumption of the continuously on comparator accounts for 63% of the total power consumption, limiting the conversion efficiency is only 34%, as shown in Fig. 3(b), even though the power consumption of the reference voltage can be reduced to 10-nA order [11].

To improve the conversion efficiency in the sleep mode, a clocked hysteresis control (CHC) buck converter with a power-law frequency scaling scheme is proposed in this paper. Replacing the continuously on comparator used in conventional hysteresis control by a clocked comparator, as shown in Fig. 2(b) [12], the buck converter consumes no dc current in the comparators. The proposed power-law frequency scaling scheme dynamically adjusts the clock frequency for the clocked comparator depending on the load current to stabilize the output voltage. As a result, the comparator power consumption becomes proportional to the load current. The buck converter can achieve almost flat conversion efficiency over the whole load current range specified by BLE while inheriting a quick wakeup response of hysteresis control. This paper is organized as follows. Section II describes the system architecture of the proposed CHC buck converter employing a power-law frequency scaling scheme operating in DCM. The power-law frequency scaling scheme, including the frequency stability, the output voltage ripple, and the effect of the load fluctuation, is analyzed in Section III. Circuit implementations are illustrated in Section IV. Experimental results are shown in Section V. Finally, conclusion is presented in Section VI.

## II. SYSTEM ARCHITECTURE

A system block diagram of the proposed CHC buck converter is shown in Fig. 4. The target input voltage ranges

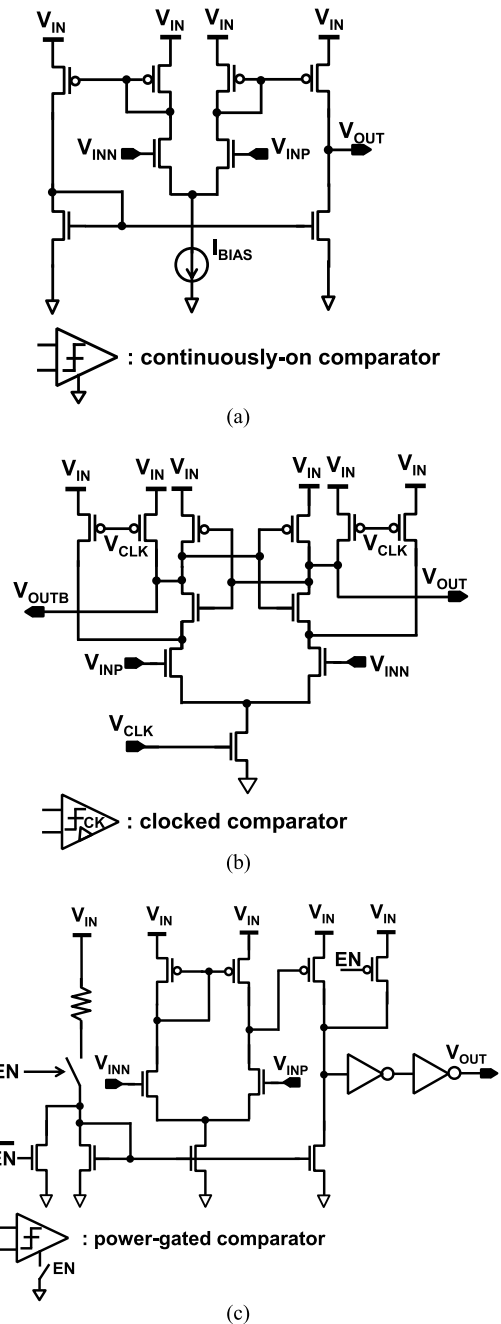


Fig. 2. Circuit schematic and symbol of comparator. (a) Continuously on comparator. (b) Clocked comparator. (c) Power-gated comparator. (This topology is used in Fig. 4.)

from 2.4 to 3.3 V, allowing it to be a battery-based system. The output voltage is set to be 1.5–1.6 V to power LSI circuits in sensor nodes with BLE communication. For typical sensor node applications, the buck converter operates in DCM because of the low load current while using an inductor with small inductance. Compared with the conventional hysteresis buck converter, the continuously on comparator is replaced by a clocked comparator  $X_1$ . Comparators  $X_2$  and  $X_3$  are power-gated comparators whose circuit schematic and symbol are shown in Fig. 2(c). We note that for  $X_3$ , a topology consisting of a pMOS input differential pair with an nMOS active load is

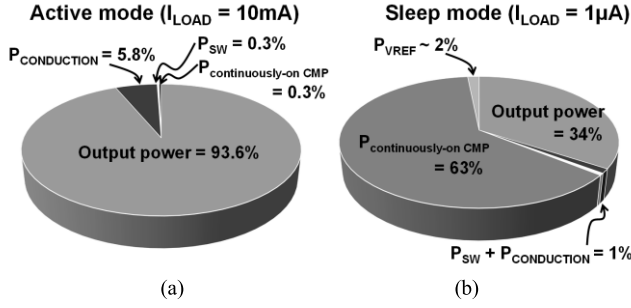


Fig. 3. Simulated power dissipation of typical hysteresis buck converter in active and sleep modes. (a) Active mode. (b) Sleep mode.  $P_{CONDUCTION}$  and  $P_{SW}$  denote the conduction and switching losses of the converter, respectively.  $P_{VREF}$  denotes the power consumption of a reference voltage generator  $V_{REF}$ .

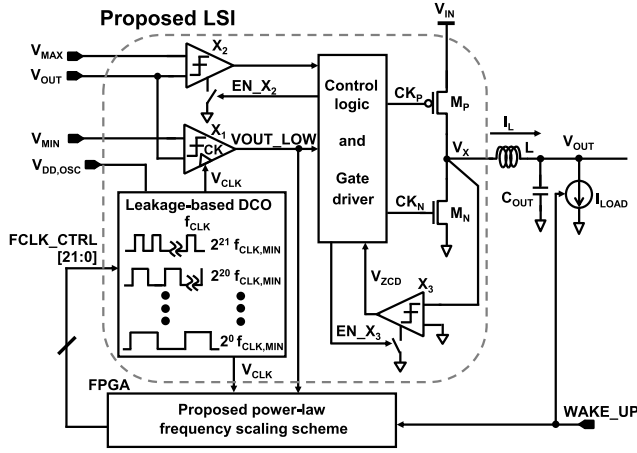


Fig. 4. System block diagram of the proposed CHC buck converter with power-law frequency scaling scheme.

applied because  $X_3$  compares  $V_X$  with ground. Using an enable signal,  $X_2$  and  $X_3$  are turned ON in a short period of time in every switching cycle. The bias points of the current mirror and the output are reset to ground and logic “1,” respectively, by the enable signal EN. Therefore, no dc current is consumed when the comparators are disabled.  $X_1$  and  $X_2$  are designed to regulate  $V_{OUT}$  within a hysteresis voltage window specified by voltage references  $V_{MAX}$  and  $V_{MIN}$ . The dependence of the output voltage ripple on the hysteresis voltage window will be discussed in Section III. In addition, comparator  $X_3$  is used for zero-current detection (ZCD), preventing reverse inductor current loss.  $X_3$  compares  $V_X$  with ground and generates a signal to turn OFF the nMOS power transistor  $M_N$  when the inductor current reaches zero. An analog-type comparator is necessary because  $X_2$  and  $X_3$  should operate sufficiently quickly to reduce the output voltage ripple and to prevent reverse inductor current, respectively. Since there is no need for  $X_2$  and  $X_3$  to be turned ON all the time, they are activated for a short time when the enable signal for each comparator is ON.

A leakage-based digitally controlled oscillator (DCO) is implemented to provide a clock signal  $V_{CLK}$  to  $X_1$ . The frequency of  $V_{CLK}$ ,  $f_{CLK}$ , can be adjusted from  $2^0 f_{CLK,MIN}$  to  $2^{21} f_{CLK,MIN}$  by 22-bit clock frequency control signals named  $F_{CLK\_CTRL}$  [21:0], where  $f_{CLK,MIN}$  denotes the lowest clock frequency.  $F_{CLK\_CTRL}$  [21:0] are provided by a

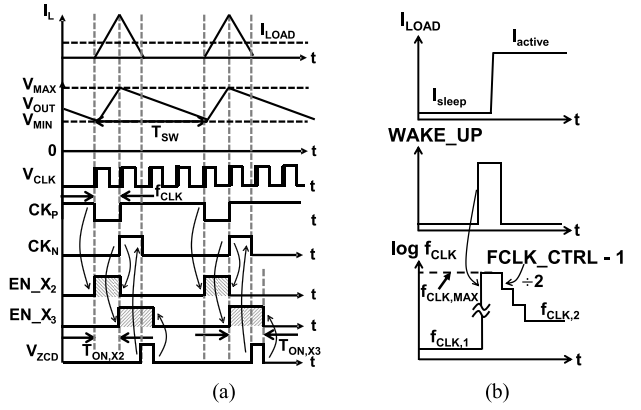


Fig. 5. (a) Operating timing diagram and relative control signals in CHC buck converter. (b) Load wakeup operation.

field-programmable gate array (FPGA) for an experiment but can easily be implemented on a chip. The power-law frequency scaling scheme is implemented by the FPGA.  $V_{CLK}$  and the output signal of  $X_1$ ,  $V_{OUT\_LOW}$ , are applied to the FPGA to generate  $F_{CLK\_CTRL}$ . If  $f_{CLK}$  is too slow considering the load condition,  $F_{CLK\_CTRL}$  is increased by 1 bit, making  $f_{CLK}$  double. On the other hand, if  $f_{CLK}$  is too fast for the load condition,  $F_{CLK\_CTRL}$  is decreased by 1 bit, making  $f_{CLK}$  a half. The exact meanings of “too slow” and “too fast” are described later. Therefore,  $f_{CLK}$  is controlled in accordance with the load conditions. Only basic logic elements are used on the FPGA. By a simple calculation [13], the employed gate count on the FPGA is about 700 gates, which consume less than 1 nW when  $I_{LOAD}$  is 500 nA,  $f_{CLK}$  is 15 Hz, and  $V_{IN}$  is 3 V, which is negligible compared with the power loss in a sleep mode.

Fig. 5(a) shows the operating timing diagram of the proposed CHC buck converter. When  $V_{OUT}$  becomes lower than  $V_{MIN}$ , which is detected by  $X_1$ ,  $V_{OUT\_LOW}$  is logic “1” and pMOS power transistor  $M_P$  is turned ON, which conducts an inductor current and charges up the output voltage. At the same time, comparator  $X_2$  is enabled and starts comparing  $V_{OUT}$  with  $V_{MAX}$ . Once  $V_{OUT}$  reaches  $V_{MAX}$ ,  $M_P$  is turned OFF and nMOS power transistor  $M_N$  is turned ON. The turn-ON signal for  $M_N$  is also used to disable  $X_2$  and enable  $X_3$ .  $M_N$  is turned OFF when the inductor current reaches zero, which is detected by the ZCD comparator  $X_3$ .  $X_3$  is disabled automatically when  $M_N$  is turned OFF.  $X_2$  and  $X_3$  are turned ON during  $T_{ON,X2}$  and  $T_{ON,X3}$ , respectively, in every power stage switching period  $T_{SW}$ . Therefore, applying the proposed control scheme, comparators  $X_1$ ,  $X_2$ , and  $X_3$  are all “clocked” and consume no dc power.

The conduction and switching losses in the buck converter are estimated as follows:

$$P_{conduction} = I_{L,RMS}^2 \cdot (R_{DS,ON} + R_{ESR}) \quad (1)$$

$$P_{switching} = \alpha \cdot f_{SW} \cdot C_{TOTAL} \cdot V_{IN}^2 \quad (2)$$

where  $I_{L,RMS}$  is the root mean square of the inductor current,  $R_{DS,ON}$  is the ON resistance of power transistors  $M_P$  and  $M_N$ ,  $R_{ESR}$  is the equivalent series resistance of the inductor,  $f_{SW}$  is the switching frequency of the power stage,  $V_{IN}$  is the

input voltage,  $C_{TOTAL}$  is the total capacitance at the gates of  $M_P$  and  $M_N$ , and  $\alpha$  is the average activity factor. In addition, the power consumption of  $X_2$  and  $X_3$  can also be estimated as

$$P_{comp.,X2,3} = \frac{1}{T_{SW}} \int_0^{T_{ON,X2,3}} V_{IN} I(t) dt \quad (3)$$

where  $1/T_{SW}$  is the switching frequency of the power stage  $f_{SW}$ ,  $T_{ON,X2}$ , and  $T_{ON,X3}$  are the turn-ON time of comparators  $X_2$  and  $X_3$ , respectively, and  $I(t)$  is the current consumed by the comparator. As indicated in (1)–(3), by adopting PFM in DCM operation, the conduction loss, switching loss, and power consumption of  $X_2$  and  $X_3$  can be scaled with  $I_{LOAD}$  because all of them are proportional to  $f_{SW}$ . The power consumption of clocked comparator  $X_1$ , however, is proportional to the clock frequency  $f_{CLK}$ . An appropriate clock frequency is required to regulate the output voltage while keeping the power consumption of  $X_1$  low. Using a higher clock frequency results in higher power consumption of  $X_1$  and the controller circuits, thus losing the benefit of using the clocked comparator. On the other hand, applying a lower clock frequency induces a large voltage ripple at  $V_{OUT}$ . A power-law frequency scaling scheme is proposed to adjust the clock frequency  $f_{CLK}$  in the CHC buck converter, making  $f_{CLK}$  also proportional to  $I_{LOAD}$ . Therefore, the conduction loss and switching loss of the power stage, and the controller power consumption including the comparators are all scaled with  $I_{LOAD}$ . Thus, the CHC buck converter can achieve almost flat conversion efficiency over a wide range of loads including a sleep mode.

For IoT sensor node applications, the buck converter must support quick wakeup operation when the system operation changes from a sleep mode to an active mode. The wakeup operation of the CHC buck converter is illustrated in Fig. 5(b). The load current as the wakeup threshold can be set depending on applications for power and output voltage drop optimization. When the system is woken up, an external wakeup signal  $WAKE\_UP$  synchronized with a change in  $I_{LOAD}$  is applied to the FPGA or a controller on the chip if the logic is implemented on a chip. The current frequency control bits,  $F_{CLK\_CTRL}$  [21:0], are reset by  $WAKE\_UP$ , making  $f_{CLK}$  changes from the current frequency  $f_1$  to the highest frequency  $f_{CLK,MAX}$ , that is,  $2^{21} f_{CLK,MIN}$ . With the proposed frequency scaling scheme, the clock frequency  $f_{CLK}$  gets half and half step by step, and automatically settles to a new value  $f_2$  according to the loading condition. Therefore, the buck converter can achieve fast wakeup operation.

### III. POWER-LAW FREQUENCY SCALING SCHEME

A flowchart of the proposed frequency scaling scheme is shown in Fig. 6. At the start of the control, the clock frequency  $f_{CLK}$  is set to the highest value,  $2^{21} f_{CLK,MIN}$ , and the  $V_{OUT}$  checking counter implemented on the FPGA is reset to 0. If  $V_{OUT} > V_{MIN}$  at the clock edge, meaning that  $V_{OUT\_LOW}$  is logic “0,” the counting number  $n$  increases by 1, and the process restarts. On the other hand, if  $V_{OUT} < V_{MIN}$  at the clock edge,  $V_{OUT\_LOW}$  is logic “1,” making the buck converter starts a new switching cycle. At the same time, the counter number

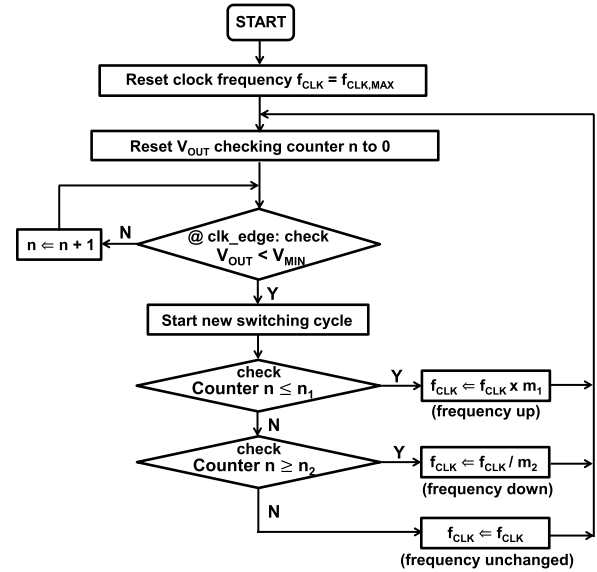


Fig. 6. Frequency control flowchart of the proposed frequency scaling scheme.

TABLE I  
FREQUENCY SCALING OF  $f_{CLK}$  AND DEPENDENCE OF  $f_{CLK}$  ON  $I_{LOAD}$  EXPRESSED USING  $n$ ,  $n_1$ , AND  $n_2$

$V_{OUT}$ checking counter $n$ @ $V_{OUT} < V_{MIN}$	Current $f_{CLK}$ @ $I_{LOAD}$	Frequency multiply/divide
$n \leq n_1$	Too low	$\times m_1$
$n_2 > n > n_1$	Appropriate	unchanged
$n \geq n_2$	Too high	$\div m_2$

$n$  is read out and compared with two preset boundaries,  $n_1$  and  $n_2$ , where  $n_2 > n_1$ .  $n \leq n_1$  indicates that the output voltage  $V_{OUT}$  crosses  $V_{MIN}$  earlier than expected, that is,  $I_{LOAD}$  is high but the clock frequency  $f_{CLK}$  is too low.  $M_P$  should be turned ON frequently to transfer energy from  $V_{IN}$  to  $V_{OUT}$ . Therefore,  $f_{CLK}$  is multiplied by  $m_1$  and the algorithm restarts.  $n > n_1$  and  $n > n_2$  mean that  $f_{CLK}$  is too high. Clocked comparator  $X_1$  checks  $V_{OUT}$  several times and turns ON  $M_P$  only once. In this case,  $f_{CLK}$  is divided by  $m_2$ . This process operates continuously, and the  $V_{OUT}$  checking counter number  $n$  settles to a value larger than  $n_1$  and smaller than  $n_2$ , i.e.,  $n_2 > n > n_1$ . In the steady state, an appropriate  $f_{CLK}$  is found by the proposed power-law frequency scaling scheme that can stabilize the output voltage of the buck converter, and  $f_{CLK}$  is a multiple of the switching frequency  $f_{SW}$ . Therefore, the power consumption of  $X_1$  is also proportional to  $I_{LOAD}$  because  $f_{CLK}$  is proportional to  $f_{SW}$ . These three conditions of  $n$  including the frequency scaling and the relation between  $f_{CLK}$  and  $I_{LOAD}$  are summarized in Table I. An example of implementation showing the output waveform, the clock signal,  $V_{OUT\_LOW}$ , and the  $V_{OUT}$  checking counter  $n$  in the time domain when  $m_1 = m_2 = 2$ ,  $n_1 = 2$ , and  $n_2 = 5$  is illustrated in Fig. 7. In Fig. 7(a),  $V_{OUT}$  is lower than  $V_{MIN}$  when  $n = 2 \leq n_1$  in the first switching period. This is the case when the initial  $f_{CLK}$  is too low possibly generating a larger output voltage ripple. Thus,  $f_{CLK}$  is doubled ( $\times m_1$ ). On the

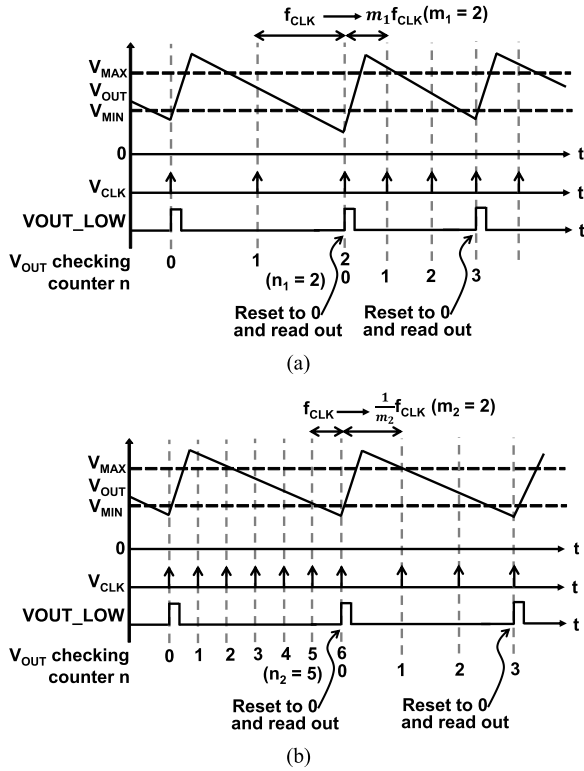


Fig. 7. (a) When the initial  $f_{CLK}$  is too low,  $f_{CLK}$  is doubled. (b) When the initial  $f_{CLK}$  is too high,  $f_{CLK}$  is halved.

other hand, when the initial  $f_{CLK}$  is too high,  $V_{OUT}$  is lower than  $V_{MIN}$  when  $n > n_2$ , resulting in the consumption of more power than appropriate, which is the case shown in Fig. 7(b).  $f_{CLK}$  becomes halved ( $\div m_2$ ) to reduce the power consumption of the comparator. In Sections III-A–III-C, the design parameters that make the CHC buck converter works properly are determined. Then, the frequency stability, the output voltage ripple, and the effect of the load current fluctuation on  $V_{OUT}$  are derived theoretically.

#### A. Frequency Multiply/Divide Ratio Decision

Parameters  $m_1$ ,  $m_2$ ,  $n_1$ , and  $n_2$  illustrated in Fig. 6 should be determined to make the frequency scaling scheme operates properly. As indicated by Fig. 6,  $f_{CLK}$  can be expressed as

$$f_{CLK} = \frac{m_1^q}{m_2^p} f_{CLK,MIN} \quad (4)$$

$$m_1 = m_2^\gamma \quad (5)$$

where  $p$  and  $q$  denote the corresponding decision cycles and  $m_1$ ,  $m_2$ ,  $p$ , and  $q$  are natural numbers. Considering that the frequency scaling scheme may induce harmonics that interfere with other sensitive circuits such as RF blocks on the same chip, the relation between  $m_1$  and  $m_2$  is expressed as (5), where  $\gamma$  is designed as a natural number, that is, larger than or equal to 1. Therefore, the harmonics generated by the frequency scaling scheme are located at integral multiples of  $f_{CLK,MIN}$  in the frequency spectrum. Replacing  $m_1$  in (4) by (5),  $f_{CLK}$  can be expressed as

$$f_{CLK} = m_2^N f_{CLK,MIN}, \quad N = \gamma q - p \quad (6)$$

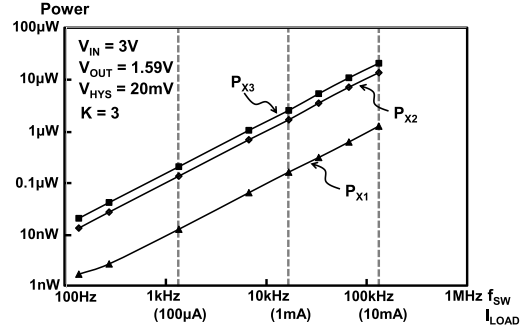


Fig. 8. Simulated dependence of power consumption of comparators ( $X_1$ ,  $X_2$ , and  $X_3$ ) on  $f_{SW}$  and  $I_{LOAD}$ .

where  $N$  is also a natural number. As indicated by (5), any natural numbers  $m_1$ ,  $m_2$ , and  $\gamma$  can be chosen for the power-law frequency scaling scheme. A higher  $m_1$  results in a high tracking speed for the  $I_{LOAD}$  wakeup operation, but dissipates more power in every frequency transition. On the other hand, a higher  $m_2$  can reduce power consumption during the transient. However, according to the analysis in Section III-C, a higher value of  $m_2$  rapidly reduces the clock frequency, which induces a large output voltage drop and an unacceptable output voltage ripple. Therefore, except 1, the minimum value of a natural number, 2, is chosen for  $m_2$ , resulting in frequency scaling of  $2^N$ . Depending on the application,  $m_1$  can be designed to be 8 or higher for a high response speed of load changing. In a sleep mode, however, a minimum value of 2 is designed for  $m_1$  to reduce the power overhead. The combination of  $(m_1, m_2) = (2, 2)$  results in double-half-frequency scaling [14], which is a special case in the proposed power-law frequency scaling scheme.

$n_1$  and  $n_2$  should be designed to prevent  $f_{CLK}$  oscillation between  $f_{CLK} \times m_1$  and  $f_{CLK} \div m_2$ . The constraints on  $n_1$  and  $n_2$  can be represented as

$$n_2 \times \frac{1}{m_2} > n_1 \quad (7)$$

$$n_1 \times m_1 > n_2. \quad (8)$$

Therefore,  $f_{CLK}$  is stable between  $n_1$  and  $n_2$ , and its relation with  $f_{SW}$  in the steady state can be expressed as

$$f_{CLK} = K \times f_{SW} \quad (9)$$

where  $K$  is a natural number and a function of  $n_1$  and  $n_2$ .  $f_{CLK}$  is determined by the power-law frequency scaling scheme according to the load conditions, making the CHC buck converter able to operate stably without  $f_{CLK}$  oscillation. Under the same  $I_{LOAD}$  condition, choosing a larger value of  $K$  results in a higher  $f_{CLK}$ . An additional benefit here compared with a conventional hysteresis control is that the switching frequency  $f_{SW}$  is fixed to  $1/K \cdot f_{CLK}$ . Using the frequency scaling scheme, the power consumption of the clocked comparator can be adjusted to be proportional to  $I_{LOAD}$ . The simulated dependence of the power consumption of  $X_1$ ,  $X_2$ , and  $X_3$  on  $f_{CLK}$  when  $K = 3$  is shown in Fig. 8. Obviously, the power consumption of  $X_1$ ,  $X_2$ , and  $X_3$  can all be scaled with  $I_{LOAD}$ .

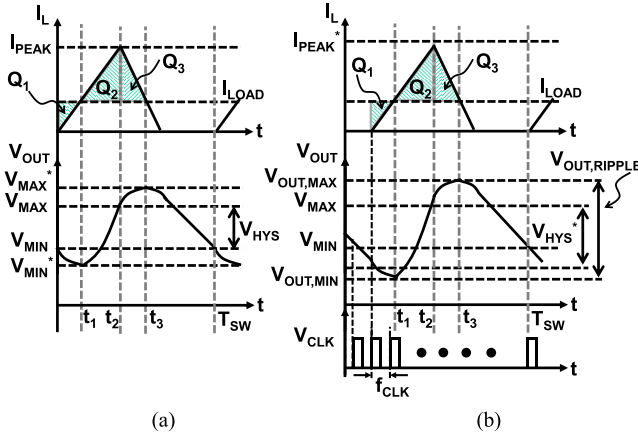


Fig. 9. Inductor current and output voltage waveforms. (a) Conventional hysteresis buck converter. (b) Proposed CHC buck converter with clock timing.

### B. Analysis of Output Voltage Ripple

By applying the proposed power-law frequency scaling scheme in the CHC, the buck converter employs no continuously on comparators, resulting in no consumption of dc current by the comparators. The output voltage ripple  $V_{OUT, RIPPLE}$ , however, is enlarged because comparator  $X_1$  only compares the output voltage with  $V_{MIN}$  at the clock edge. In addition, the “real” minimum output voltage level  $V_{OUT, MIN}$ , which is lower than  $V_{MIN}$ , should be analyzed to ensure that the lowest output voltage level is not lower than the specification value. By the proposed theoretical analysis, design guidelines for  $V_{MAX}$  and  $V_{MIN}$  are provided so that the CHC buck converter can achieve competitive performance with a conventional buck converter while improving the conversion efficiency in a sleep mode.

To analyze the voltage ripple of the CHC buck converter, the voltage ripple of conventional hysteresis control is derived first. The inductor current waveforms  $I_L$ ,  $I_{LOAD}$ , and  $V_{OUT}$  for a conventional hysteresis control buck converter are illustrated in Fig. 9(a).  $I_{PEAK}$  is the peak inductor current value,  $V_{MAX} - V_{MIN}$  is the hysteresis window, denoted by  $V_{HYS}$ , and  $I_{LOAD}$  is the load current. Because of the time delay between the inductor current and the output voltage, the maximum and minimum output voltages, denoted by  $V_{MAX}^*$  and  $V_{MIN}^*$ , are higher and lower than  $V_{MAX}$  and  $V_{MIN}$ , respectively. Therefore,  $V_{MAX}^* - V_{MIN}^*$  represents the output voltage ripple. When the output capacitor equivalent series resistance is neglected for simplicity, the peak inductor can be expressed as [15]

$$I_{PEAK} = I_{LOAD} + \sqrt{I_{LOAD}^2 + 2C_{OUT}\alpha_1 V_{HYS}} \quad (10)$$

where  $\alpha_1 = (V_{IN} - V_{OUT})/L$  and  $V_{HYS} = V_{MAX} - V_{MIN}$ . Using charge balance analysis [16] in combination with (10), the output voltage ripple can be expressed in terms of only the given specification parameters of the system such as  $V_{IN}$ ,  $V_{OUT}$ ,  $V_{HYS}$ ,  $L$ ,  $C_{OUT}$ , and  $I_{LOAD}$

$$V_{OUT, RIPPLE} = \frac{1}{2C_{OUT}} (I_{LOAD}^2 + 2C_{OUT}\alpha_1 V_{HYS}) \frac{V_{IN}}{V_{OUT}} \frac{1}{\alpha_1}. \quad (11)$$

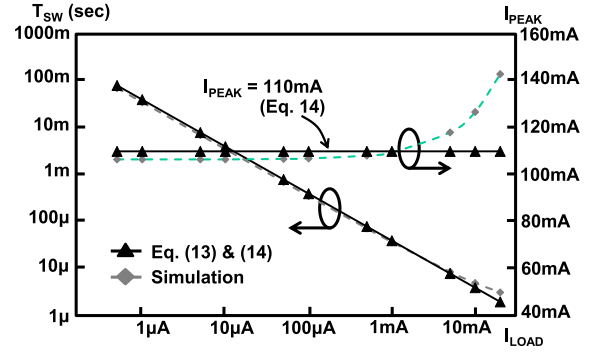


Fig. 10. Simulated and calculated  $T_{SW}$  and  $I_{PEAK}$  by (13) and (14) under different load conditions.

A similar equation can also be found in [17] although it involves the switching period and cannot refer to the specification parameters directly.

For IoT sensor node applications, the maximum  $I_{LOAD}$  usually ranges from milliamperes to 10-mA order. In this case, the  $2C_{OUT}\alpha_1 V_{HYS}$  term in (10) is much larger than  $I_{LOAD}^2$  term when a microfarad output capacitor and a microhenry inductor are applied. Therefore, (11) can be simplified to

$$V_{OUT, RIPPLE}(0) = V_{HYS} \times \frac{V_{IN}}{V_{OUT}}. \quad (12)$$

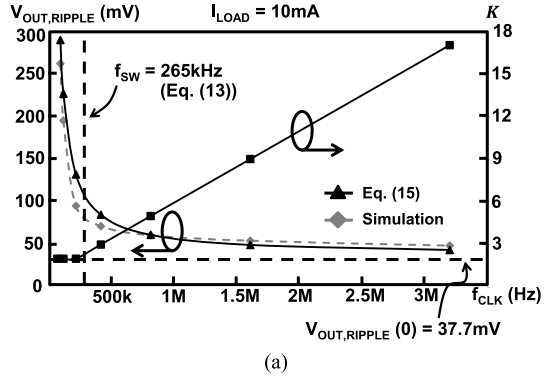
Equation (12) provides a simple estimation of the output voltage ripple that is only dependent on  $V_{IN}$ ,  $V_{OUT}$ , and  $V_{HYS}$ . Equation (12) is defined as the intrinsic output voltage ripple of a hysteresis buck converter, indicating the theoretical minimum output ripple that it can achieve. In addition, the switching period  $T_{SW}$  and  $I_{PEAK}$  can also be simplified as follows when  $\sqrt{2C_{OUT}\alpha_1 V_{HYS}} > I_{LOAD}$ :

$$T_{SW} = \frac{C_{OUT}}{I_{LOAD}} V_{HYS} \frac{V_{IN}}{V_{OUT}} \quad (13)$$

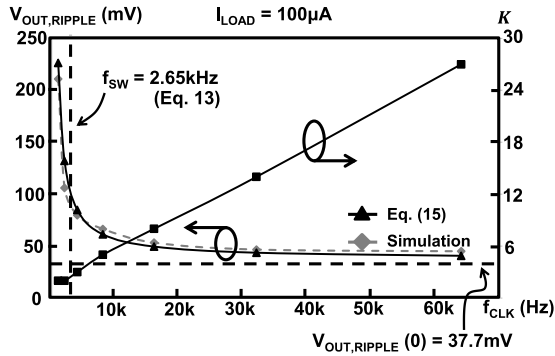
$$I_{PEAK} = \sqrt{2C_{OUT}\alpha_1 V_{HYS}}. \quad (14)$$

Equations (12)–(14) can be used to calculate the output voltage ripple, switching period, and peak inductor current very simply when the load current is relatively small compared with  $I_{PEAK}$ , which is the usual case in IoT applications. The values of  $T_{SW}$  and  $I_{PEAK}$  calculated by (13) and (14) compared with simulation results under different  $I_{LOAD}$  are shown in Fig. 10. Equations (13) and (14) match the simulation results well and provide a simple means of calculating  $T_{SW}$  and  $I_{PEAK}$  for a conventional hysteresis buck converter when  $I_{LOAD}$  is much lower than  $I_{PEAK}$ . In addition, on the basis of (12)–(14), the voltage ripple of the proposed CHC buck converter can be calculated.

Fig. 9(b) shows the inductor current waveform  $I_L$ ,  $I_{LOAD}$ ,  $V_{OUT}$ , and the clock signal  $V_{CLK}$  when CHC is applied. The clocked comparator compares  $V_{OUT}$  and  $V_{MIN}$  at every clock edge. The effective hysteresis window  $V_{HYS}^*$ , however, is enlarged by a limited clock frequency  $f_{CLK}$  and  $K$  as indicated by (9). The worst case of  $V_{OUT, RIPPLE}$  is when the clock arrives but  $V_{OUT}$  is slightly higher than  $V_{MIN}$ . Therefore,  $V_{HYS}^*$  is effectively enlarged by a factor



(a)



(b)

 Fig. 11. Simulated and calculated dependences of output voltage ripple on clock frequency  $f_{CLK}$ . (a)  $I_{LOAD} = 10$  mA. (b)  $I_{LOAD} = 100$   $\mu$ A.

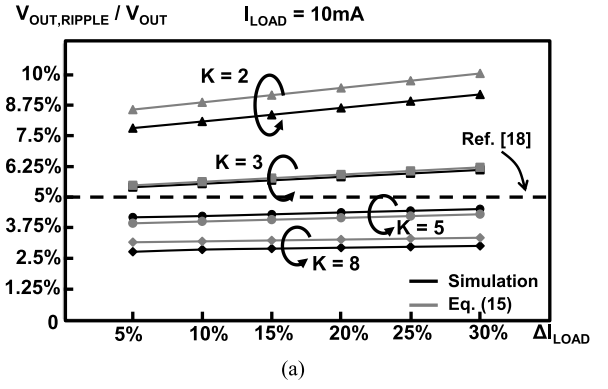
of  $T_{OSC} \times I_{LOAD}/C_{OUT}$ . Therefore,  $V_{OUT, RIPPLE}$  can be calculated as

$$V_{OUT, RIPPLE}(CHC) = \frac{V_{IN}}{V_{OUT}} (V_{HYS} + \frac{I_{LOAD}}{C_{OUT}} T_{CLK}). \quad (15)$$

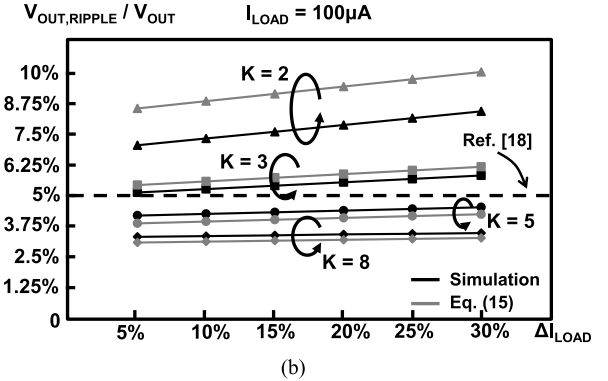
The calculated and simulated dependences of  $V_{OUT, RIPPLE}$  on  $f_{CLK}$ , including the simulated  $K$  under  $V_{IN} = 3$  V,  $V_{OUT} = 1.6$  V,  $V_{HYS} = 20$  mV,  $C_{OUT} = 1$   $\mu$ F,  $L = 4.7$   $\mu$ H, and  $I_{LOAD} = 10$  mA and  $100$   $\mu$ A, are shown in Fig. 11(a) and (b), respectively. When  $f_{CLK}$  is closed to the switching frequency  $f_{SW}$  calculated by (13), the output voltage ripple increases steeply. On the other hand, when a higher  $f_{CLK}$  is applied,  $V_{OUT, RIPPLE}$  becomes smaller and close to the intrinsic output voltage ripple calculated by (12) at the cost of higher power consumption.

### C. $V_{OUT, RIPPLE}$ and $V_{OUT, MIN}$ Under $I_{LOAD}$ Fluctuation

The lowest output voltage level  $V_{OUT, MIN}$  and the maximum voltage ripple  $V_{OUT, RIPPLE}$  of the proposed CHC buck converter under time-dependent  $I_{LOAD}$  fluctuation should be calculated. Unlike a conventional buck converter only depending on the output capacitor and the converter loop bandwidth,  $f_{CLK}$  and  $K$  determine  $V_{OUT, MIN}$  and  $V_{OUT, RIPPLE}$ . Considering that the  $I_{LOAD}$  fluctuation is not sufficiently large to change  $f_{CLK}$  to  $m_1 \times f_{CLK}$ , a large value of  $K$  is required to keep the minimum output voltage level above the system specifications. Equation (15) gives the worst ripple voltage, and  $K$  is determined by preset numbers  $n_1$  and  $n_2$ . Fig. 12(a) and (b) shows the simulated dependences of



(a)



(b)

 Fig. 12. Simulated and calculated output voltage ripple for  $I_{LOAD}$  with a fluctuation varying from 5% to 30% in a stepped manner with different values of  $K$ . (a)  $I_{LOAD} = 10$  mA. (b)  $I_{LOAD} = 100$   $\mu$ A.

the output voltage ripple performance of the proposed CHC buck converter on  $K$  under  $I_{LOAD} = 10$  mA and  $100$   $\mu$ A, respectively. The load current is assumed to have a fluctuation of up to 30%. The calculation results obtained from (15) and a PFM control with an adaptive on-time buck converter [18] are also illustrated in Fig. 12(a) and (b) for comparison. The simulation is carried out with  $V_{IN} = 3$  V,  $V_{OUT} = 1.6$  V,  $V_{HYS} = 20$  mV,  $L = 4.7$   $\mu$ H, and  $C_{OUT} = 1$   $\mu$ F. A larger value of  $K$  indicates that a higher  $f_{CLK}$  is applied as shown in Section III-A. When  $K = 2$ , the output voltage is easily affected by load fluctuation. In addition, when  $K = 3$ , the CHC buck converter achieves competitive voltage ripple performance with the adaptive on-time buck converter. Applying  $K = 5$ , the voltage ripple of the CHC buck converter is lower than that of the conventional one when the  $I_{LOAD}$  fluctuation varies from 5% to 30%. Therefore,  $K = 3$  is chosen for low-power consumption with acceptable output voltage ripple.

To ensure that the minimum output voltage is higher than the value specified by the system, the lower bound of the voltage hysteresis window  $V_{MIN}$  should be designed so that is satisfies

$$V_{OUT, MIN}(CHC) = V_{MIN} - \frac{I_{LOAD}}{C_{OUT}} T_{CLK} - \frac{Q_L}{C_{OUT}} \quad (16)$$

where  $Q_L$  can be expressed as

$$Q_L = \frac{I_{LOAD} \times t_D}{2}, \quad t_D = \frac{I_{LOAD} \times L}{V_{IN} - V_{OUT}} \quad (17)$$

and the comparator delay is neglected for simplicity. When  $I_{LOAD}$  is 10 mA,  $V_{IN} = 3$  V, and  $V_{OUT} = 1.6$  V,

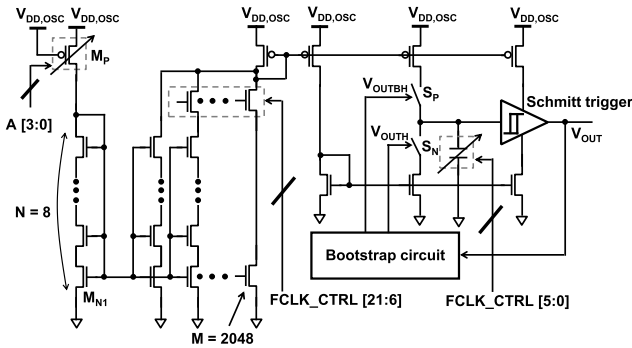


Fig. 13. Circuit schematic of the leakage-based DCO.

$V_{MIN} = 1.57$  V gives the CHC buck converter with a minimum output voltage no lower than 3.4% of  $V_{OUT}$ , and  $V_{OUT, RIPPLE} < 6\%$  of  $V_{OUT}$  when  $K = 3$ . Therefore, the design parameters  $m_1 = m_2 = 2$ ,  $n_1 = 2$ , and  $n_2 = 5$ , resulting in  $K = 3$ , which is the case shown in Fig. 7(a) and (b), are chosen to implement the proposed CHC buck converter.

#### IV. CIRCUIT IMPLEMENTATION

##### A. Leakage-Based Digitally Controlled Oscillator (DCO)

An on-chip DCO is implemented to provide a clock signal to the clocked comparator  $X_1$ . The clock frequency is able to be controlled digitally using a factor of 2 and ranges from hertz to megahertz order for both active and sleep modes. A circuit schematic of the DCO is shown in Fig. 13. As the DCO is the only continuously on circuit block in the CHC buck converter, the power consumption should be minimized so that it does not limit the sleep mode conversion efficiency. The transistor leakage current is designed as the bias current provided to the current mirror. The 4-bit signals  $A [3:0]$  are used to control the transistor size of  $M_P$  and the leakage current according to the process, voltage, and temperature (PVT) variation.  $A [3:0]$  can be generated by additional calibrations or implementing a PVT sensors on a chip [19], [20]. This current is mirrored to charge and discharge the capacitors, generating a sawtooth voltage waveform. A current-starved Schmitt trigger is used as a comparator and output buffer so that there is no need to use an additional reference. Therefore, a square clock waveform can be obtained at the output of the Schmitt trigger. The frequency tuning is separated to control both the transistor multiplier ratio and the number of capacitors. The 22-bit thermometer codes,  $F_{CLK\_CTRL} [21:0]$ , are used to adjust the clock frequency monotonically over a frequency tuning range of  $10^6$ . In addition, stacked transistor technology is employed to design  $M_{N1}$  to dramatically reduce the transistor area. Therefore, the MSB nMOS transistor multiplier ratio can be reduced to 2048, which can be implemented on a test chip.

To reduce the oscillator power consumption, a supply  $V_{DD, OSC}$  with a lower voltage is preferred. A bootstrap circuit employing the concept in [21] is designed to boost the voltage level of  $V_{OUT}$  when the Schmitt trigger is switching. Therefore, switches  $S_N$  and  $S_P$  can be fully turned ON to charge and discharge the capacitor even when  $V_{DD, OSC}$  is as

low as 0.6 V. An additional low-dropout regulator (LDO) or a switched capacitor (SC) dc-dc converter can be employed to generate this supply voltage. The measurement results show that the DCO consumes only 5.6 nA at 15 Hz and 50.4  $\mu$ A at 6 MHz when  $V_{DD, OSC}$  is 0.6 V. Therefore, it is possible to design the LDO or the SC dc-dc converter [22] on a chip with high conversion efficiency and a compact area although this has not been implemented in the current design.

The frequency scaling scheme applied to the DCO may generate interference that interferes with sensitive circuits on the chip. In the sleep mode, however, the clock frequency is only 10-Hz order, which is far from the usual RF signal frequency. In addition, there are no RF circuits enabled in the sleep mode. On the other hand, in the active mode, a system clock with a higher frequency, for example, 32 MHz, can be applied as a base frequency for the power-law frequency scaling scheme instead of using the internal leakage-based DCO.

##### B. Clocked Comparator and Analog Comparator With Enable Signal

A circuit schematic of clocked comparator  $X_1$  is shown in Fig. 2(b). A clocked comparator with a latch load [14] is employed to compare  $V_{OUT}$  with  $V_{MIN}$ . The output followed by a D flip-flop generates a control signal to turn ON the power transistor  $M_P$ . The input differential pair is designed with a large transistor width and length to reduce the offset voltage. The 1-sigma simulated and calculated offset voltages [23] are less than 2 mV, which does not have a large effect on the voltage hysteresis window.

Fig. 2(c) shows a circuit schematic of the power-gated comparator with an enable signal. Comparator  $X_2$  compares  $V_{OUT}$  with  $V_{MAX}$ , and is enabled when  $V_{OUT}$  is lower than  $V_{MIN}$  and turned OFF when  $V_{OUT}$  becomes higher than  $V_{MAX}$ . Similarly, a p-type input differential pair with an nMOS active load power-gated comparator is designed for  $X_3$  because the comparator compares the  $V_X$  node with the ground.  $X_3$  is turned ON when  $V_{OUT}$  becomes higher than  $V_{MAX}$  and turned OFF when the inductor current reaches zero. The settling time due to the enable signal in the comparators is not an issue because the bias points in the comparators only need to settle in a time of 100-ns order. To demonstrate the benefit of the proposed CHC, the power distribution of the comparators is simulated. The simulation shows that the power consumptions of  $X_1$ ,  $X_2$ , and  $X_3$  are all lower than 1% of the output power when applying  $f_{CLK} = 100$  Hz under  $I_{LOAD} = 1$   $\mu$ A.

##### C. Voltage Level Shifter

The proposed CHC buck converter targets BLE applications for which the input voltage could be a battery with a voltage ranging from 2.4 to 3.3 V. However, a lower supply voltage is preferred for the leakage-based DCO to reduce the power consumption. A conventional level shifter with a short current reduction topology [24] cannot convert a clock signal with a low voltage such as 0.6–3.3 V when the clock frequency is in the megahertz order. Fig. 14 shows the designed voltage level shifter. An auxiliary bootstrap circuit is designed to

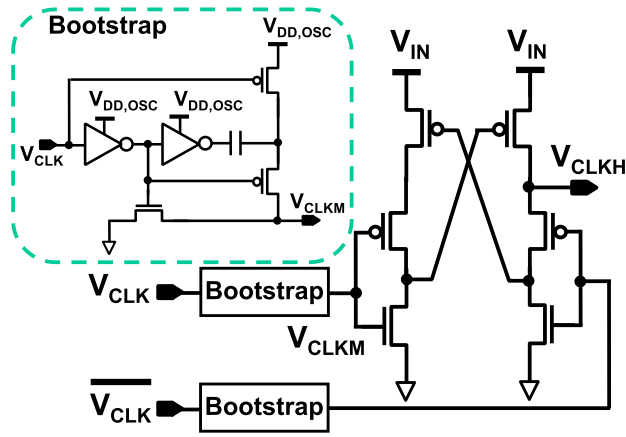


Fig. 14. Schematic of the voltage level shifter, which converts 0.6–3.3 V with the frequency ranging from 1 Hz to 5 MHz.

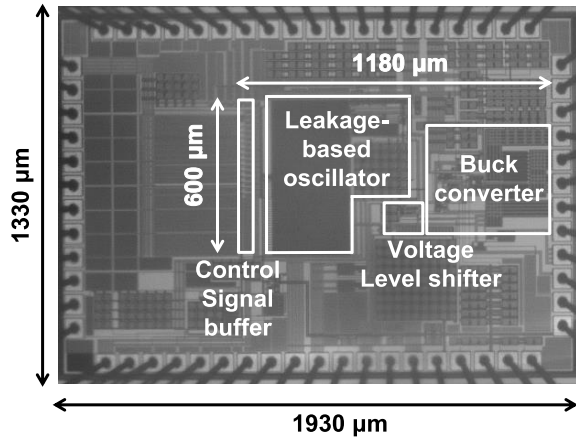


Fig. 15. Chip micrograph of the proposed CHC buck converter.

boost the amplitude of the input clock signal  $V_{CLK}$  to nearly  $2V_{DD,OSC}$  ( $\sim 1.2$  V), and the voltage level shifter can shift  $V_{CLKM}$  to  $V_{CLKH}$  functionally. The worst case is when the clock frequency is low. In this case, the bootstrap circuit cannot boost the input voltage for a long period. Simulation results show that the voltage level shifter can convert the input signal from 0.6 to 3.3 V when the frequency ranges from 1 Hz to 5 MHz. The voltage level shifter consumes 380 pW at 1 Hz and 44.5  $\mu$ W at 5 MHz.

## V. EXPERIMENTAL RESULTS

The proposed CHC buck converter implemented with the double-half-frequency scaling scheme ( $m_1 = 2$  and  $m_2 = 2$ ) is fabricated by a 0.18- $\mu$ m standard CMOS process for verification. I/O transistors are used to design buck converter core circuits that should withstand an input voltage of 3.3 V, and switches providing a low leakage current. Fig. 15 shows the chip micrograph. The active area including the buck converter core circuits, leakage-based DCO, voltage level shifter, and buffers is 0.71 mm<sup>2</sup>. The test chip is measured with a 4.7- $\mu$ H off-chip inductor and a 1- $\mu$ F off-chip capacitor, and the frequency scaling scheme is realized using an Altera Cyclone V FPGA. Fig. 16(a) and (b) shows the

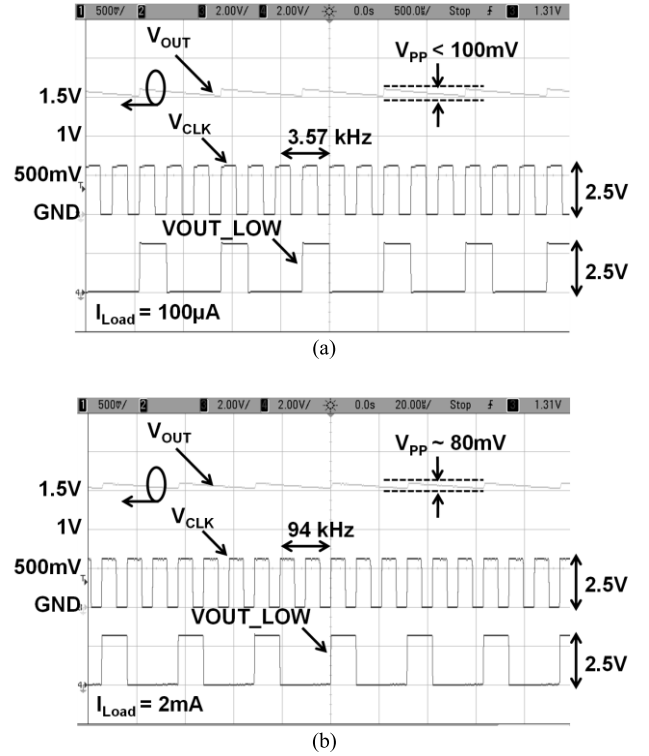


Fig. 16. Measured waveforms of  $V_{OUT}$ ,  $V_{CLK}$ , and  $V_{OUT\_LOW}$  under different loading conditions. (a)  $V_{IN} = 3$  V,  $V_{OUT} = 1.6$  V,  $V_{HYS} = 20$  mV, and  $I_{LOAD} = 100$   $\mu$ A. (b)  $V_{IN} = 3$  V,  $V_{OUT} = 1.6$  V,  $V_{HYS} = 20$  mV, and  $I_{LOAD} = 2$  mA.

steady-state waveforms of  $V_{OUT}$ ,  $V_{CLK}$ , and  $V_{OUT\_LOW}$  under  $V_{IN} = 3$  V,  $V_{MIN} = 1.57$  V, and  $V_{MAX} = 1.59$  V when  $I_{LOAD} = 100$   $\mu$ A and 2 mA, respectively. The voltage hysteresis window  $V_{HYS}$  is set to 20 mV for all measurements. The frequency scaling scheme is designed to minimize the power consumption of the comparator and controller. Therefore,  $n_1 = 2$  and  $n_2 = 5$  are used, resulting in  $K = 3$  in (9). As shown in Fig. 16, the pMOS power transistor  $M_P$  is turned ON every three  $V_{CLK}$  clock cycles. As discussed in Section III,  $m_1$ ,  $m_2$ ,  $n_1$ , and  $n_2$  can be changed easily according to the specifications for different applications, such as a high wakeup response speed or a low output voltage ripple. The measurement results show that the output voltage is regulated at 1.6 V with a voltage ripple lower than 100 mV, which is about 6% of the output voltage. Using the frequency scaling scheme, the clock frequency of  $V_{CLK}$  automatically settles to 3.57 and 94 kHz when  $I_{LOAD} = 100$   $\mu$ A and 2 mA, respectively.

To verify the load wakeup operation,  $I_{LOAD}$  changed from 30  $\mu$ A to 2 mA is applied to the output. The signal  $WAKE\_UP$  resets the clock frequency to the highest value, and the clock frequency is settled in the steady state by the frequency scaling scheme as shown in Fig. 17(a). Fig. 17(b) shows the detailed waveforms of  $V_{OUT}$ ,  $V_{CLK}$ , and  $WAKE\_UP$ . The clock frequency changes from 780 Hz to 55 kHz at 2-mA loading without an obvious voltage drop.

Fig. 18 shows the measured clock frequency and power consumption versus  $F_{CLK\_CTRL}$  [21:0] for the leakage-based

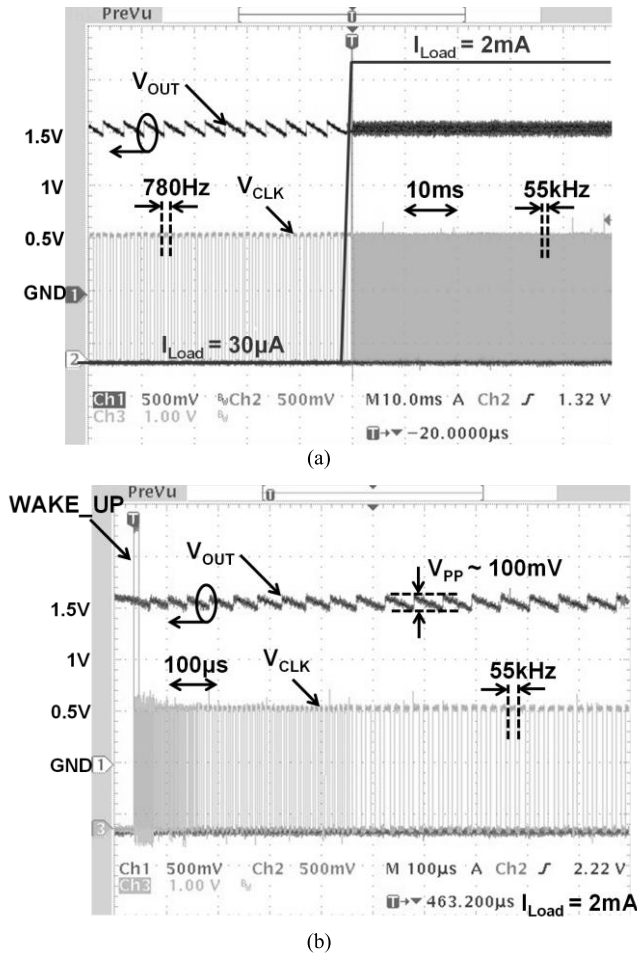


Fig. 17. Measured load wakeup operation when  $I_{LOAD}$  is changed from a sleep mode ( $30 \mu\text{A}$ ) to an active mode ( $2 \text{ mA}$ ). (a) Time scale =  $10 \text{ ms}$ . (b) Time scale =  $100 \mu\text{s}$ .

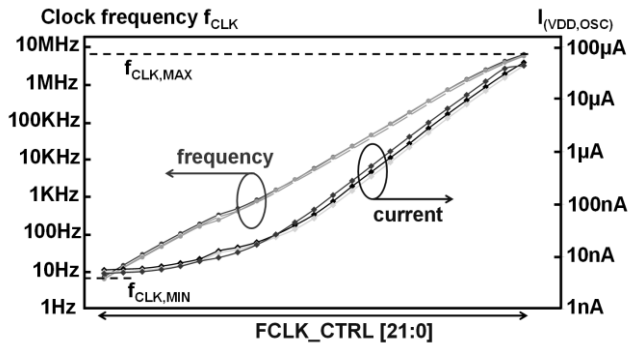


Fig. 18. Measured clock frequency and power consumption relationship for the proposed DCO in Fig. 13 when digital bit of  $F_{CLK\_CTRL}$  is changed.

DCO. The clock frequency is controlled by a 22-bit thermometer code with 16 bits in the transistor multiplier ratio and 6 bits in the capacitor bank. Three chips are measured, showing that the frequency can be adjusted monotonically without large frequency and power variations. Upon applying a  $0.6\text{-V}$  supply voltage, the DCO consumes  $3.4 \text{ nW}$  and  $30.2 \mu\text{W}$  when the clock frequency is  $15 \text{ Hz}$  and  $6.3 \text{ MHz}$ , respectively. In addition, the DCO power consumption is also

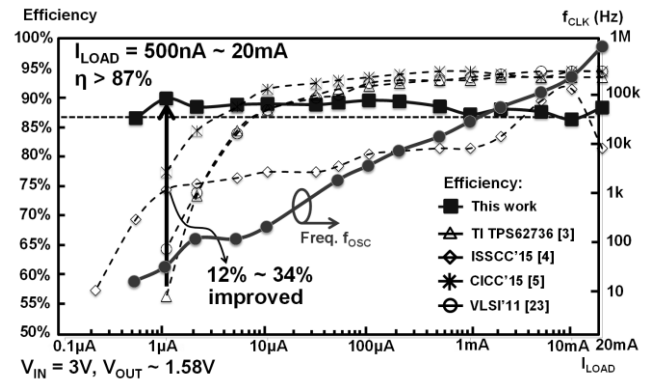


Fig. 19. Measured conversion efficiency and clock frequency  $f_{CLK}$  versus  $I_{LOAD}$  and comparison with state-of-the-art low-power buck converters.

TABLE II  
PERFORMANCE SUMMARY OF THE PROPOSED CHC BUCK CONVERTER AND COMPARISON WITH STATE-OF-THE-ART BUCK CONVERTERS

	ISSCC'15 [4]	CICC'15 [5]	VLSI'15 [6]	VLSI'11 [25]	This work
Technology	180nm CMOS	350nm CMOS	180nm CMOS	250nm CMOS	180nm CMOS
Die size	$1.44 \text{ mm}^2$	$2.88 \text{ mm}^2$	$2.42 \text{ mm}^2$	$0.21 \text{ mm}^2$	$0.71 \text{ mm}^2$ *
$V_{IN}$ (V)	0.6/1.2	2.2–6	3	1.2–2.5	2.4–3.3
$V_{OUT}$ (V)	0.35–0.5	2.5	1	1	1.5–1.6
$I_{LOAD}$	100nA–20mA	1μA–100mA	10nA–1μA	1μA–100mA	500nA–20mA
Peak eff. $\eta_{PEAK}$	92%	95%	87%	95.2	90.4%
$\eta$ @ $I_{LOAD}=1\mu\text{A}$	75%	78%	87%	65%	90.4%
Inductor value L	$4.7\mu\text{H}$	$2.2\mu\text{H}$	$47\mu\text{H}$	$1.5\mu\text{H}$	$4.7\mu\text{H}$
Control methodology	PWM, PFM, and AM	Hysteresis control	Constant on-time	Dynamic on/off time	Clocked hysteresis control

\* Active area

proportional to the loading current because the frequency is mainly controlled by the transistor multiplier ratio in the current mirror. The power distribution of the DCO accounts for less than 1% of the output power of the CHC buck converter when operating in both the sleep and the active modes.

The measured dependence of the efficiency and clock frequency  $f_{CLK}$  on the load current is shown in Fig. 19. The proposed CHC buck converter achieves almost flat conversion efficiency by removing continuously on comparators and applying the double-half-frequency scaling scheme. The frequency scaling scheme is also verified on the y-axis on the right-hand side of Fig. 19. Higher than 87% conversion efficiency is achieved over a load current ranging from  $500 \text{ nA}$  to  $20 \text{ mA}$ . When  $I_{LOAD} = 1 \mu\text{A}$ , which is defined as the sleep current in BLE, efficiency is improved by 12%–34% compared with that of state-of-the-art low-power buck converters. A comparison of performance with state-of-the-art buck converters is shown in Table II. The proposed CHC buck converter achieves higher than 87% conversion efficiency over  $500 \text{ nA}$ – $20 \text{ mA}$  with a peak efficiency of 90.4%. In addition, compared with the state-of-the-art buck converters, a higher efficiency at  $1 \mu\text{A}$  is also achieved. The input voltage, output voltage, and loading current are designed for

BLE applications. CHC with the double-half-frequency scaling scheme was also proposed to remove the continuously on comparators in the conventional hysteresis buck converter. The frequency scaling scheme is also suitable for other converters that employ continuously on comparators.

## VI. CONCLUSION

A CHC buck converter operating in DCM with a power-law frequency scaling scheme is developed to remove the continuously on comparators used in conventional hysteresis control, resulting in no dc current being consumed by the comparators. The frequency of the clocked comparator is dynamically adjusted in accordance with the load conditions. Therefore, the conduction loss, switching loss, and comparator power consumption in the converter can all be scaled with the load. By applying the proposed topology, the CHC buck converter achieves almost flat conversion efficiency over the entire load current range. The frequency stability, output voltage ripple, and minimum output voltage level of the buck converter when the power-law frequency scaling scheme is applied are analyzed to provide design guidelines for the system. A CHC buck converter with the double-half-frequency scaling scheme is implemented to verify the power-law frequency scaling. Experimental results demonstrate that the buck converter achieves conversion efficiency of higher than 87% over  $I_{LOAD}$  ranging from 500 nA to 20 mA with a peak value of 90.4%. The conversion efficiency is particularly improved when  $I_{LOAD}$  is 1  $\mu$ A. The  $I_{LOAD}$  wakeup operation with the frequency scaling scheme is also verified. The proposed buck converter achieves high conversion efficiency in a sleep mode with a quick wakeup response, making it extremely suitable for IoT sensor node applications.

## REFERENCES

- [1] M. Lueders *et al.*, "Architectural and circuit design techniques for power management of ultra-low-power MCU systems," *IEEE Trans. Very Large Scale Integr. (VLSI) Syst.*, vol. 22, no. 11, pp. 2287–2296, Nov. 2014.
- [2] *Bluetooth Low Energy*. Accessed: Jun. 2010. [Online]. Available: <https://www.bluetooth.com>
- [3] Texas Instrument. (2013). *Programmable Output Voltage Ultra-Low Power Buck Converter With up to 50 mA/200 mA Output Current*, TPS62736 Datasheet. [Online]. Available: <http://www.ti.com/lit/ds/symlink/tps62736.pdf>
- [4] P.-H. Chen, C.-S. Wu, and K.-C. Lin, "A 50 nW-to-10 mW output power tri-mode digital buck converter with self-tracking zero current detection for photovoltaic energy harvesting," *IEEE J. Solid-State Circuits*, vol. 51, no. 2, pp. 523–532, Feb. 2016.
- [5] D. Lu, S. Yao, and B. Shao, "A 110nA quiescent current buck converter with zero-power supply monitor and near-constant output ripple," in *Proc. IEEE Custom Integr. Circuits Conf. (CICC)*, Sep. 2015, pp. 1–4.
- [6] D. El-Damak and A. P. Chandrakasan, "Solar energy harvesting system with integrated battery management and startup using single inductor and 3.2 nW quiescent power," in *Proc. IEEE Symp. VLSI Circuits*, Jun. 2015, pp. 280–281.
- [7] C. Ni and T. Tetsuo, "Adaptive constant on-time (D-CAPTM) control study in notebook applications," Texas Instrum., Dallas, TX, USA, Appl. Rep. SLVA281B, Jul. 2007.
- [8] R. Redl and J. Sun, "Ripple-based control of switching regulators—An overview," *IEEE Trans. Power Electron.*, vol. 24, no. 12, pp. 2669–2680, Dec. 2009.
- [9] G. A. Rincon-Mora, "Accurate, fast, and user programmable hysteretic comparator," U.S. Patent 6229350 B1, May 8, 2001.
- [10] F. Su, W.-H. Ki, and C.-Y. Tsui, "Ultra fast fixed-frequency hysteretic buck converter with maximum charging current control and adaptive delay compensation for DVS applications," *IEEE J. Solid-State Circuits*, vol. 43, no. 4, pp. 815–822, Apr. 2008.

- [11] T. Someya, K. Matsunaga, H. Morimura, T. Sakurai, and M. Takamiya, "56-Level programmable voltage detector in steps of 50mV for battery management," in *Proc. IEEE Asian Solid-State Circuits Conf. (A-SSCC)*, Nov. 2016, pp. 49–52.
- [12] S. Babayan-Mashhadi and R. Lotfi, "Analysis and design of a low-voltage low-power double-tail comparator," *IEEE Trans. Very Large Scale Integr. (VLSI) Syst.*, vol. 22, no. 2, pp. 343–352, Feb. 2014.
- [13] National Instruments. *FPGA Fundamentals*. Accessed: May 2012. [Online]. Available: <http://www.ni.com/white-paper/6983/en/#>
- [14] C.-S. Wu, M. Takamiya, and T. Sakurai, "Buck converter with higher than 87% efficiency over 500 nA to 20 mA load current range for IoT sensor nodes by clocked hysteresis control," in *Proc. IEEE Custom Integr. Circuits Conf. (CICC)*, Apr./May 2017, pp. 1–4.
- [15] W. Fu, S. T. Tan, M. Radhakrishnan, R. Byrd, and A. A. Fayed, "A DCM-only buck regulator with hysteretic-assisted adaptive minimum-on-time control for low-power microcontrollers," *IEEE Trans. Power Electron.*, vol. 31, no. 1, pp. 418–429, Jan. 2016.
- [16] K. K.-S. Leung and H. S.-H. Chung, "Dynamic hysteresis band control of the buck converter with fast transient response," *IEEE Trans. Circuits Syst. II, Exp. Briefs*, vol. 52, no. 7, pp. 398–402, Jul. 2005.
- [17] W.-H. Ki, K.-M. Lai, and C. Zhan, "Charge balance analysis and state transition analysis of hysteretic voltage mode switching converters," *IEEE Trans. Very Large Scale Integr. (VLSI) Syst.*, vol. 58, no. 5, pp. 1142–1153, May 2011.
- [18] B. Sahu and G. A. Rincon-Mora, "An accurate, low-voltage, CMOS switching power supply with adaptive on-time pulse-frequency modulation (PFM) control," *IEEE Trans. Circuits Syst. I, Reg. Papers*, vol. 54, no. 2, pp. 312–321, Feb. 2007.
- [19] S.-W. Chen, M.-H. Chang, W.-C. Hsieh, and W. Hwang, "Fully on-chip temperature, process, and voltage sensors," in *Proc. IEEE Int. Symp. Circuit Syst. (ISCAS)*, May 2010, pp. 897–900.
- [20] H. V. Nguyen and Y. Kim, "32 nm FinFET-based 0.7-to-1.1 V digital voltage sensor with 50 mV resolution," in *Proc. IEEE Int. Conf. IC Design Technol. (ICICDT)*, May 2012, pp. 1–4.
- [21] A. M. Abo and P. R. Gary, "A 1.5-V, 10-bit, 14.3-MS/s CMOS pipeline analog-to-digital converter," *IEEE J. Solid-State Circuits*, vol. 34, no. 5, pp. 599–606, May 1999.
- [22] H.-P. Le, S. R. Sanders, and E. Alon, "Design techniques for fully integrated switched-capacitor DC-DC converters," *IEEE J. Solid-State Circuits*, vol. 46, no. 9, pp. 2120–2131, Sep. 2011.
- [23] P. R. Gray, P. J. Hurst, S. H. Lewis, and R. G. Meyer, *Analysis and Design of Analog Integrated Circuits*, 4th ed. New York, NY, USA: Wiley, 2001.
- [24] L. T. Clark, "A high-voltage output buffer fabricated on a 2 V CMOS technology," in *Symp. VLSI Circuits, Dig. Techn. Papers*, Jun. 1999, pp. 61–62.
- [25] C.-Y. Hsieh *et al.*, "A battery-free 225 nW buck converter for wireless RF energy harvesting with dynamic on/off time and adaptive phase lead control," in *Proc. IEEE Symp. VLSI Circuits*, Jun. 2011, pp. 242–243.



**Chung-Shiang Wu** (S'14) received the B.S. degree in power mechanical engineering and the M.S. degree in electronics engineering from National Tsing Hua University, Hsinchu, Taiwan, in 2007 and 2009, respectively. He is currently working toward the Ph.D. degree in electrical engineering and information systems at the University of Tokyo, Tokyo, Japan.

From 2013 to 2015, he was a Project Researcher at the National Chiao Tung University, Hsinchu, Taiwan, where he conducted research on power management and energy harvesting integrated circuits. In 2016, he joined ON Semiconductor, Tokyo, Japan, and in 2017, the IBM T. J. Watson Research Center, New York, NY, USA, as an intern. His current research interests include power management and energy harvesting ICs, low-power mixed-signal circuits, and isolated power supply for power-electronic gate drivers.



**Makoto Takamiya** (S'98–M'00–SM'14) received the B.S., M.S., and Ph.D. degrees in electronics engineering from the University of Tokyo, Tokyo, Japan, in 1995, 1997, and 2000, respectively.

In 2000, he joined NEC Corporation, Tokyo, Japan, where he was engaged in the circuit design of high-speed digital large-scale integration. In 2005, he joined the University of Tokyo, where he is currently an Associate Professor at the VLSI Design and Education Center. From 2013 to 2014, he was a Visiting Scholar at the University of California,

Berkeley, CA, USA. His current research interests include the integrated power management circuits for the ultralow-power Internet-of-Things applications and the digital gate driver circuits for an insulated-gate bipolar transistor.

Dr. Takamiya received the 2009 and 2010 IEEE Paul Rappaport Awards and the Best Paper Award at the 2013 IEEE Wireless Power Transfer Conference. He is a member of the Technical Program Committee of the IEEE International Solid-State Circuits Conference and the IEEE Symposium on VLSI Circuits.



**Takayasu Sakurai** (S'77–M'78–SM'01–F'03) received the Ph.D. degree in electrical engineering from the University of Tokyo, Tokyo, Japan, in 1981.

In 1981, he joined Toshiba Corporation, Kawasaki, Japan, where he designed CMOS dynamic random access memory, static random access memory, reduced instruction set computers processors, DSPs, and system-on-chip solutions. He has worked extensively on interconnect delay and capacitance modeling known as Sakurai model and alpha power-law MOS model. From 1988 to 1990, he was a Visiting Researcher at the University of California, Berkeley, CA, USA, where he conducted research in the field of very large-scale integration (VLSI) computer-aided design. Since 1996, he has been a Professor at the University of Tokyo, where he is involved in low-power high-speed VLSI, memory design, interconnects, ubiquitous electronics, organic IC's and large-area electronics. He has authored/coauthored over 600 technical publications including 100 invited presentations and several books and filed over 200 patents.

Dr. Sakurai was a recipient of the 2010 IEEE Donald O. Pederson Award in Solid-State Circuits, the 2009 and 2010 IEEE Paul Rappaport award, the 2010 IEICE Electronics Society Award, the 2009 IEICE Achievement Award, the 2005 IEEE ICICDT Award, the 2004 IEEE Takuo Sugano Award, and the 2005 P&I patent of the year award and four product awards. He is an Executive Committee Chair for VLSI Symposia and a Steering Committee Chair for the IEEE A-SSCC. He served as a Conference Chair for the Symposium on VLSI Circuits and ICICDT, a Vice Chair for ASPDAC, a TPC Chair for the A-SSCC, and VLSI Symposium, an Executive Committee Member for ISLPED, and a Program Committee Member for ISSCC, CICC, A-SSCC, DAC, ESSCIRC, ICCAD, ISLPED, and other international conferences. He delivered keynote speech at over 50 conferences including ISSCC, ESSCIRC, and ISLPED. He was an Elected AdCom Member for the IEEE Solid-State Circuits Society and an IEEE CAS and SSCS Distinguished Lecturer. He is also a Domain Research Supervisor for nanoelectronics area in Japan Science and Technology Agency. He is an IEICE Fellow.